

## Control of an underwater biomimetic vehicle using Floquet theory

Nicolas Plamondon and Meyer Nahon\*

*Center for Intelligent Machines, McGill University, Montreal, Quebec, Canada*

*(Received August 12, 2014, Revised September 4, 2014, Accepted September 12, 2014)*

**Abstract.** Aqua is an underwater biomimetic vehicle designed and built at McGill University that uses six paddles to produce control and propulsion forces. It has the particularity of having time-periodic thrust due to its oscillating paddles. Using an existing model of the vehicle, two types of controller were developed: a PD controller and a Floquet controller. The Floquet controller has the advantage of explicitly addressing the time-periodicity of the system. The performance of the controllers was assessed through simulation and experimentally in the Caribbean Sea. We find that the vehicle was able to follow the prescribed trajectories with relative accuracy using both controllers, though, the Floquet controller slightly outperforms the PD controller. Furthermore, a key advantage of the Floquet controller is that it requires no tuning while the PD controller had to be tuned by trial and error.

**Keywords:** biomimetic; underwater vehicle; Floquet theory; control

---

### 1. Introduction

Conventional underwater vehicles can generally be categorized into two types: autonomous underwater vehicles (AUVs) and remotely operated vehicles (ROVs). The former are usually streamlined vehicles intended for long distance operation while the latter are bluff and omnidirectional. All these vehicles are actuated using propeller-based thrusters. Aqua, shown in Fig. 1, is an amphibious vehicle that can swim underwater or at water surface using flexible oscillating paddles or walk on land using semi-circular legs. Aqua does not fall into either of the two conventional categories of underwater vehicles mentioned above. Rather, it can be classified as a biomimetic autonomous underwater vehicle (BAUV). Among its key advantages are the ability to walk on land, to swim in the water and to be deployed from the beach. Moreover, because of its propulsion system, it can hover and change its orientation in the vertical plane without any translational movement.

Much research has been done on the control of conventional underwater robots. Yoerger and Slotine (1985) and Xu *et al.* (2001) used sliding mode theory to develop robust trajectory tracking controllers for an underwater robot. These controllers had the advantage of dealing directly with nonlinearities and being robust to an imprecise model. However, they also showed that the performance of the controllers is greatly improved by a more accurate model. Smallwood and

---

\*Corresponding author, Professor, E-mail: [meyer.nahon@mcgill.ca](mailto:meyer.nahon@mcgill.ca)

Whitcomb (2004) compared the ability of several controllers to track a prescribed trajectory. Their controllers were tested on a conventional underwater robot as well as in simulation. They found that the model-based controllers were capable of providing exact trajectory tracking. The PD controller was able to provide velocity tracking but failed to track the position accurately, though the position error remained bounded. Furthermore, they found that increasing the PD gains improved the tracking performance.

Some researchers have considered the guidance and control of biomimetic vehicles. Guo and Joeng (2004) developed a waypoint tracking controller, for a vehicle with oscillating tail fin propulsion, based on hierarchical local and global controllers so as to mimic fish behavior. The performance of the controller was evaluated in simulation with good results. They also discussed the effect of model uncertainties and disturbances on the control performance. Geder *et al.* (2008) developed a fuzzy logic PID controller to control the trajectory of a vehicle with two pectoral fins. Naik and Singh (2007) studied the motion control of a fish-like robot in the yaw plane. The motion of the vehicle is controlled by altering the motion of pectoral-like fins. They used an adaptive control law and obtained good tracking results. Plamondon and Nahon (2009) used a PID and two model-based controllers to provide trajectory tracking capabilities to an underwater biomimetic vehicle. They found that the model-based controllers outperform the PID.

Aqua has the particularity of using oscillating fins to produce its thrust. A direct consequence of this propulsion system is that the thrust is not constant but time-periodic. As a result, we can treat Aqua as a time-periodic system, and Floquet control theory is specifically aimed at the control of such systems. A number of researchers have studied the theory of time-periodic systems and some have developed methods to use Floquet theory to design controllers for these systems. Calico and Weisel (1984) developed a method based on Floquet theory allowing a determination of the location of the poles of the system. Montagnier *et al.* (2004) studied various techniques to develop controllers using Floquet theory, but this study was theoretical, rather than applied. Aho (2001) used  $H_\infty$  to design tracking controllers for a time-periodic system. He obtained good results but his technique did not deal with the time-periodicity of the system directly.

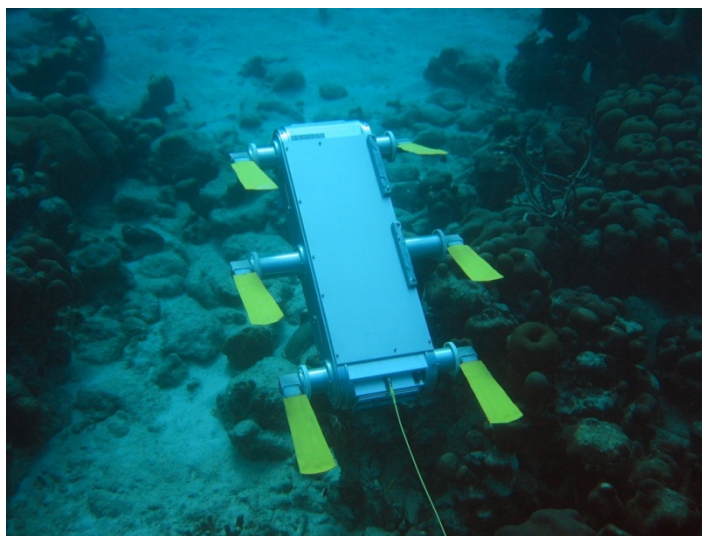


Fig. 1 Aqua underwater vehicle

Conventional control laws were applied to the Aqua vehicle with some success (Plamondon and Nahon 2006, 2009) but they assumed that the thrust was not oscillating. In order to obtain better results, we are interested in studying control laws that take into account the time-varying thrust. The objective of this research is to apply Floquet control theory to the Aqua underwater vehicle in order to develop trajectory tracking controllers. Moreover, since Floquet theory requires a linear description of the system, a linearization technique had to be developed to account for the time-varying thrust.

## 2. Dynamics model

The robot has six degrees of freedom, and we consider two relevant reference frames of interest. The first one,  $R_V$ , is the robot frame and has its origin at the centre of mass of the robot. As shown in Fig. 2, the x-axis points toward the front of the vehicle, the z-axis toward the center of the Earth and the y-axis follows the right-hand rule convention. The second one,  $R_I$ , is the inertial coordinate frame and has its origin at a fixed arbitrary point on the water surface. Euler angles ( $\phi$ ,  $\theta$ ,  $\psi$ ) are the angles between the  $R_I$  and  $R_V$  coordinate frames, where  $\phi$  is the roll angle,  $\theta$  the pitch angle and  $\psi$  the yaw angle (Fossen 1994). The motion of the robot in the 6 degrees of freedom can then be described by the following variables

$$\mathbf{n}_1 = [X \ Y \ Z]^T, \quad \mathbf{n}_2 = [\phi \ \theta \ \psi]^T, \quad \mathbf{s} = [X \ Y \ Z \ \phi \ \theta \ \psi]^T \quad (1)$$

$$\mathbf{v}_1 = [u \ v \ w]^T, \quad \mathbf{v}_2 = [p \ q \ r]^T, \quad \mathbf{v} = [u \ v \ w \ p \ q \ r]^T \quad (2)$$

where  $X$ ,  $Y$  and  $Z$  represent the position of the robot's mass center relative to the origin of the inertial frame. The velocity of the robot is expressed as components in  $R_V$ :  $u$ ,  $v$  and  $w$  are the translational velocity components, while  $p$ ,  $q$  and  $r$  are the angular velocity components.

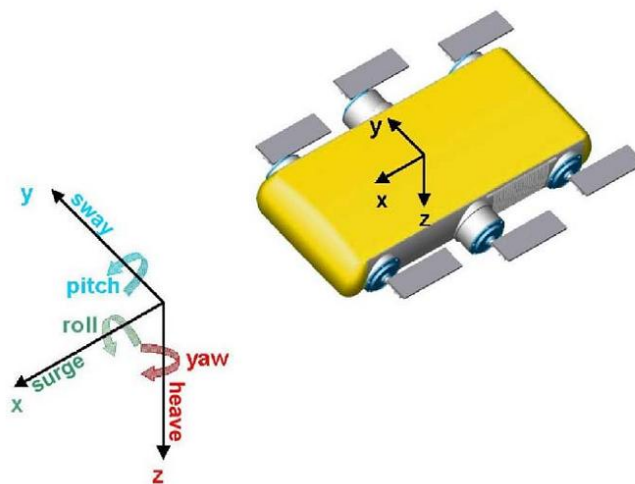


Fig. 2 Six degrees of freedom of the vehicle

### 2.1 Body model

The body model of Aqua is based on work done by Georgiades *et al.* (2009) and Fossen (1994). It takes into account the Coriolis forces, the hydrodynamic forces and the vehicle inertia

$$\mathbf{f} = \mathbf{M}\dot{\mathbf{v}} + \mathbf{C}(\mathbf{v})\mathbf{v} + \mathbf{D}(\mathbf{v})\mathbf{v} + \mathbf{g}(\mathbf{n}_2) + \mathbf{b}(\mathbf{n}_2)$$

$$\mathbf{f} = [F_x \quad F_y \quad F_z \quad M_x \quad M_y \quad M_z]$$
 (3)

where  $\mathbf{f}$  is the vector of net forces and moments produced by the paddles in the six degrees of freedom,  $\mathbf{M}$  is 6 x 6 mass matrix including added mass,  $\mathbf{C}(\mathbf{v})$  is the 6 x 6 Coriolis matrix,  $\mathbf{D}(\mathbf{v})$  is the 6 x 6 hydrodynamic matrix,  $\mathbf{g}$  is the gravitational force vector and  $\mathbf{b}$  is the buoyancy force vector. In the simulation, it is assumed that the vehicle is neutrally buoyant and the centre of gravity is coincident with the centre of buoyancy. As a result, the buoyant and gravity forces cancel each other. In practice, they are never exactly coincident because the mass distribution changes depending on which batteries, set of paddles and other pieces of equipment are installed. Since the robot is immersed in water, the Coriolis and mass matrices include a rigid body and an added mass component. The rigid body part can be understood as the mass of the robot in a vacuum, while the added mass part models added inertia due to the acceleration of the fluid. According to Fossen (1994), assuming that there are three planes of symmetry and that the vehicle is moving at low speed, the mass matrix including the rigid-body and added mass is diagonal. The hydrodynamic matrix is also a diagonal matrix. However, the Coriolis matrix  $\mathbf{C}(\mathbf{v})$  has off-diagonal terms and is responsible for the coupling between the 6 degrees of freedom. Moreover, the Coriolis and hydrodynamic matrices contain the velocity vector. As a result, these two terms are responsible for the nonlinearity of the system. The parameters in the matrices were obtained using empirical results for a solid rectangular prism (Fossen 1994). More information about the vehicle model can be found in (Plamondon and Nahon 2006, 2009).

A simulation based on Eq. (3) was implemented in MATLAB Simulink to evaluate the performance of the vehicle. It takes the paddle motion as the input and outputs the complete state of the vehicle as a function of time. It was originally developed by Georgiades *et al.* (2009) and later modified to solve our particular problem.

### 2.2 Paddle model

The paddle model consists of the relationship between the forces produced by the paddle and the paddle motion and is described in detail in (Plamondon and Nahon 2009). It computes the lift and drag forces generated by the paddle, assuming the paddle to be a tapered flat plate at a known incidence to the flow. The forces are resolved to find the propulsive thrust as shown in Fig. 3. Averaging these forces over time, we find the following relation between paddle motion and thrust:

$$Q = 0.1963 \frac{(w_1 + 2w_2)l^2}{3} \rho \frac{A}{P} - 0.1554$$
 (4)

where  $A$  and  $P$  are the amplitude and period of the paddle oscillations respectively;  $l$ ,  $w_1$  and  $w_2$  are the paddle length and width at each end; and  $\rho$  is the water density. This model was developed

from fundamental principles and calibrated using experimental data obtained from paddle tests in a tank. Eq. (4) is then used to create a reverse model that determines the best combination of  $A$  and  $P$  to produce a desired thrust (Plamondon and Nahon 2009). This reverse model is based on an optimization where we try to keep  $A$  and  $P$  close to desired values.

### 3. Linearization

The dynamics model described in Section 2 is nonlinear. Although it is convenient for a simulation of the vehicle a linear model is necessary for the design of the Floquet controller (Section 4).

The general nonlinear model of the Aqua vehicle can be written as  $\dot{\mathbf{x}} = \mathbf{F}(\mathbf{x}, \mathbf{f})$ , where  $\mathbf{f}$  is as defined in Eq. (3), which oscillates at twice the frequency of oscillation of the paddle and  $\mathbf{x}$  is the state vector defined as  $[\mathbf{v}^T \mathbf{s}^T]^T$ . The linear model would then take the following form

$$\dot{\mathbf{x}} = \mathbf{A}\mathbf{x} + \mathbf{B}\mathbf{f} \quad (5)$$

where  $\mathbf{A}$  is a  $12 \times 12$  matrix and  $\mathbf{B}$  is a  $12 \times 6$  matrix.  $\mathbf{A}$  is defined as

$$\mathbf{A} = \frac{\partial \mathbf{F}}{\partial \mathbf{x}} = \begin{bmatrix} \frac{\partial F_1}{\partial x_1} & \frac{\partial F_1}{\partial x_2} & \dots & \frac{\partial F_1}{\partial x_{12}} \\ \frac{\partial F_2}{\partial x_1} & \frac{\partial F_2}{\partial x_2} & \dots & \frac{\partial F_2}{\partial x_{12}} \\ \vdots & \vdots & \ddots & \vdots \\ \frac{\partial F_{12}}{\partial x_1} & \frac{\partial F_{12}}{\partial x_2} & \dots & \frac{\partial F_{12}}{\partial x_{12}} \end{bmatrix} \quad (6)$$

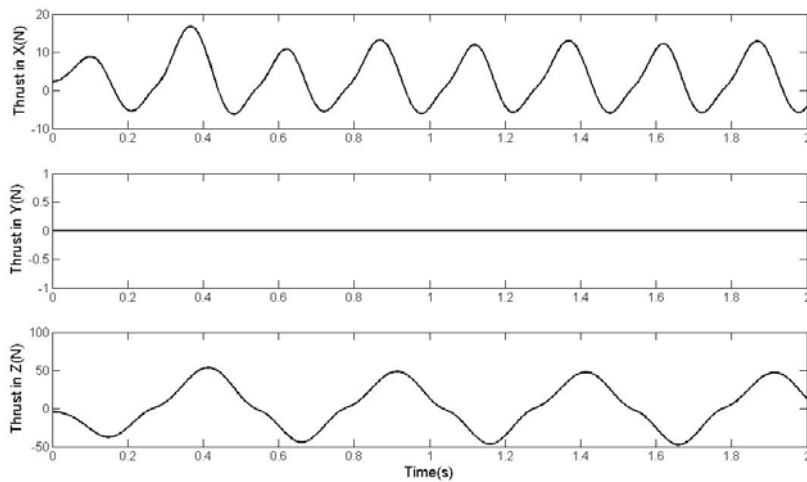


Fig. 3 Thrust acting on centre of gravity of the robot for  $A = 0.6 \text{ rad}$  and  $P = 0.5 \text{ s}$

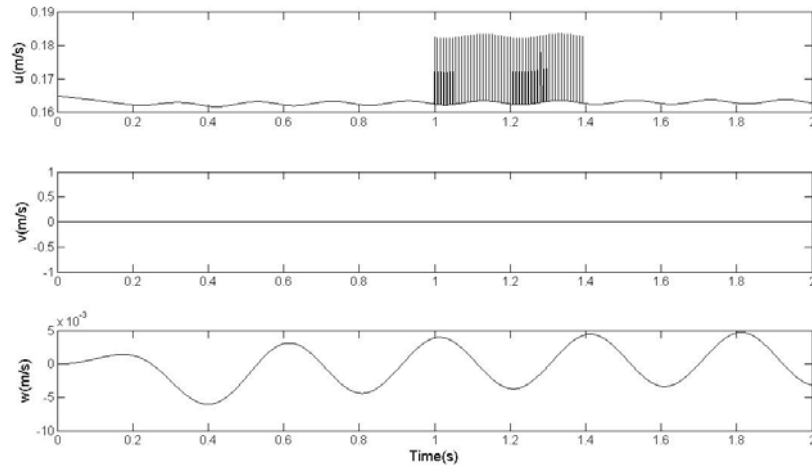


Fig. 4 Disturbance in the surge velocity for  $u = 0.16 \text{ m/s}$  for  $A = 0.6 \text{ rad}$  and  $P = 0.4 \text{ s}$

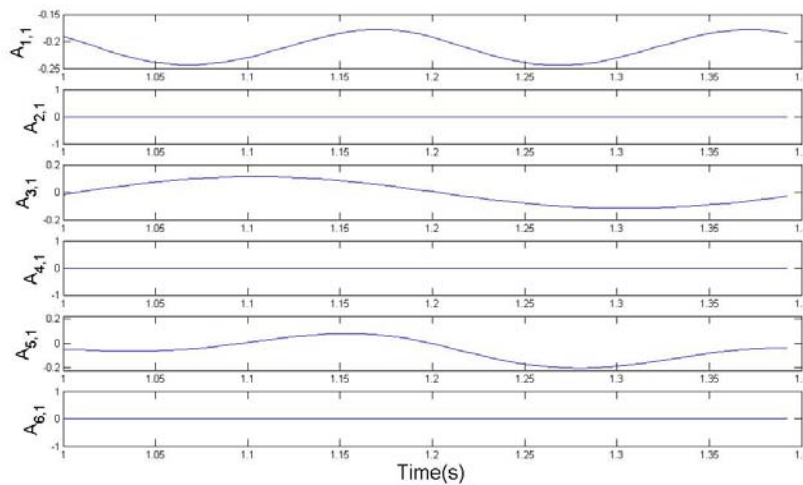


Fig. 5 Response to a disturbance of  $0.016 \text{ m/s}$  in  $u$  for  $A = 0.6 \text{ rad}$  and  $P = 0.4 \text{ s}$

There are several methods that can be used to linearize a nonlinear time-invariant system about an equilibrium operating point; for example, numerical differentiation by finite difference. Because Aqua has oscillating thrust as shown in Fig. 3, it will never reach an equilibrium point and will instead oscillate around a steady-state value. This precludes the direct use of a finite difference approach and an alternative method was designed to account for the unsteady equilibrium. A disturbance was applied at regular interval over one period of oscillation as can be seen in Fig. 4. For the specific case shown in Fig. 4, the nominal steady-state condition is  $u = 0.16$

m/s with all other velocities equal to zero. A disturbance of 0.016 m/s is applied to  $u$ , 20 times over the paddle cycle. The response of the system in the six degrees of freedom, for the disturbance shown in Fig. 4, is shown in Fig. 5. This corresponds to the first six rows of the first column of the state matrix  $\mathbf{A}$ . Rows 7-12 are not displayed because the bottom left part of matrix  $\mathbf{A}$  is a 6-by-6 identity matrix. We can see that for a disturbance in  $u$  as shown in Fig. 4, there is a response in surge, heave and pitch motion but not in the other three degrees of freedom as shown in Fig. 5. We can also notice that the surge motion oscillates at twice the paddle frequency while the heave and pitch motion oscillate at the paddle frequency.

The total value of  $A_{ij}$  is composed of two parts: one constant and one oscillating,  $A_{ij}(t) = \bar{A}_{ij}(t) + A_{ij}(t)$ , as is apparent from Fig. 5. The average entries of matrix  $\mathbf{A}$  can be computed from the average response to a disturbance

$$\bar{A}_{ij} = \frac{\text{average}(\Delta \dot{x}_i)}{\Delta x_j} \quad (7)$$

The RMS value of  $\bar{A}_{ij}$  was calculated to evaluate the periodic variation of the dynamics of the robot. Fig. 6 shows the average value and RMS value of the first column of state-matrix  $\mathbf{A}$  for the disturbance shown in Fig. 5. We found that the diagonal elements had the largest average values of all entries. Moreover, the constant part is more important than its RMS counterpart except in the case where the average is close to zero, such as  $A_{3,1}$  shown in Figs. 5 and 6.

#### 4. Floquet controller

Floquet theory is a branch of the theory of ordinary differential equation that allows the solution of time-periodic problems. It is named after Gaston Floquet, a French mathematician, and its main result is a coordinate change that transforms a time-periodic system into a linear time-invariant system. It can also be used to design controllers for time-periodic systems. As noted earlier, Aqua uses oscillating paddles to propel itself through water, resulting in a thrust is periodic at twice the paddle frequency.

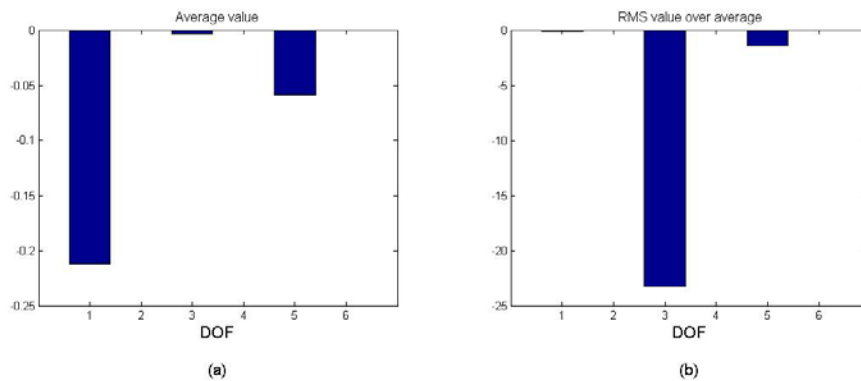


Fig. 6 (a) Average value of Fig. 5 and (b) RMS over average value of Fig. 5

As a result of the periodic nature of the system, Floquet-Lyapunov theory seems a good candidate for the development of controllers for the Aqua vehicle. A linear model for the vehicle can be represented as follows

$$\begin{aligned}\dot{\mathbf{x}}(t) &= \mathbf{A}(t)\mathbf{x}(t) + \mathbf{B}(t)\mathbf{u}(t) \\ \mathbf{y}(t) &= \mathbf{C}(t)\mathbf{x}(t)\end{aligned}\quad (8)$$

where  $\mathbf{A}(t)$ ,  $\mathbf{B}(t)$  and  $\mathbf{C}(t)$  are the time-periodic state-space linear matrices with period  $P$ ,  $\mathbf{x}(t)$  is the state vector and  $\mathbf{u}(t)$  is the input vector. Some elements of the state-space matrices oscillate with period  $0.5P$ , but they are still  $P$ -periodic.

The linear model presented in Eq. (8) is valid for all systems and not specific to our vehicle. In the particular case of Aqua, it is important to note that matrix  $\mathbf{A}$  depends on time and on velocity. During the linearization process discussed in Section 3, the vehicle was linearized for different velocities. As a result, matrix  $\mathbf{A}(t)$  presented in Eq. (8) is exact only for the particular velocity used in the linearization process. In the case where the velocity of the vehicle was to change significantly during the operation, gain scheduling should be used.

The solution to the homogenous equation, with no input  $\mathbf{u}(t)$  is given by

$$\mathbf{x}(t) = \mathbf{\Phi}(t, t_0)\mathbf{x}(t_0) \quad (9)$$

where  $\mathbf{\Phi}(t, t_0)$  is the state-transition matrix and must satisfy the following differential equation

$$\frac{d\mathbf{\Phi}(t, t_0)}{dt} = \mathbf{A}(t)\mathbf{\Phi}(t, t_0) \quad (10)$$

The results presented in Eqs. (8)-(10) are analogous to those of conventional linear theory, with the exception that  $\mathbf{A}(t)$ ,  $\mathbf{B}(t)$  and  $\mathbf{\Phi}(t, t_0)$  are periodic instead of constant. The main result of Floquet theory is that the state-transition matrix can be factored into two matrices  $\mathbf{F}$  and  $\mathbf{J}$

$$\mathbf{\Phi}(t, t_0) = \mathbf{F}(t)e^{\mathbf{J}t}\mathbf{F}^{-1}(t_0) \quad (11)$$

where  $\mathbf{J}$  is a constant matrix and  $\mathbf{F}(t)$  a time-varying matrix. These two matrices are often called the Floquet factors. There are several methods to obtain the matrices  $\mathbf{F}(t)$  and  $\mathbf{J}$  and it is important to note that there are many possible solutions to this problem. However, the eigenvalues of  $\mathbf{J}$ , called the Poincaré exponents ( $\omega_i$ ), are unique. Solving a Floquet problem for all time requires determining the constant matrix  $\mathbf{J}$  and the time-periodic matrix  $\mathbf{F}(t)$  for one full period. We now discuss methods to obtain the state-transition matrix and the Floquet factors.

#### 4.1 Computation of state-transition matrix

The state-transition matrix is used to obtain the general solution of a linear dynamics system governed by Eq. (8). The state-transition matrix allows calculation of the state of the system at time  $t$  from the state at time  $t_0$  as shown by Eq. (9). In our case, the state-transition matrix is used to obtain the Floquet factors in Section 4.2.

Cai *et al.* (2001) developed an alternative method to calculate  $\mathbf{x}(t)$  that allows finding the state-transition matrix in a single pass. Effectively, their method solves a system of the form

$$\frac{d\mathbf{x}(t)}{dt} = \mathbf{A}_0\mathbf{x}(t) + (\mathbf{A}(t) - \mathbf{A}_0)\mathbf{x}(t) \quad (12)$$

where  $\mathbf{A}_0$  is the constant part of  $\mathbf{A}(t)$  and  $(\mathbf{A}(t) - \mathbf{A}_0)$  can be expressed as

$$(\mathbf{A}(t) - \mathbf{A}_0) = \sum (\mathbf{D}_c \sin(ct) + \mathbf{B}_c \cos(ct)) \quad (13)$$

where  $\mathbf{D}_c$  and  $\mathbf{B}_c$  are constant coefficient matrices and  $c$  are the frequencies of the system. In our case, the system oscillates at a single frequency (twice the paddle frequency) but in other situations, there could be more than one frequency, hence the summation sign. Then, after some manipulation, Cai *et al.* (2001) developed an equation to find the vector  $\mathbf{x}(t)$  from the previous time step

$$\mathbf{x}_{k+1} = \mathbf{H}_{k+1}\mathbf{x}_k \quad (14)$$

where  $\mathbf{H}_{k+1}$  is a matrix that updates the state  $\mathbf{x}_k$  into  $\mathbf{x}_{k+1}$ .

The monodromy matrix can then found from:

$$N = \frac{T}{\Delta t} \rightarrow \Phi(T, 0) = \prod_{n=1}^N \mathbf{H}_{k-n+1} \quad (15)$$

By choosing a small enough step size, the discrete state-transition matrix given by Eq. (15) can be considered continuous.

#### 4.2 Floquet factors using the eigenvalues and eigenvectors

This section describes a technique to compute the Floquet factors from the state-transition matrix found in Section 4.1. It is derived from direct observation of Eq. (11) and its similarity to an eigenvalue problem. In the current form of the equation, there are two unknowns ( $\mathbf{J}$  and  $\mathbf{F}(t)$ ) and it is therefore impossible to solve the eigenvalue problem. We evaluate Eq. (11) after one period in order to circumvent this problem. If we assume that  $\mathbf{F}(t)$  is periodic with period  $P$  then  $\mathbf{F}(P + t_0) = \mathbf{F}(t_0)$ , and evaluation of Eq. (11) at  $t = P$  gives us

$$\Phi(P, 0) = \mathbf{F}(0)e^{\mathbf{J}P}\mathbf{F}^{-1}(0) \quad (16)$$

Because the system is time-periodic we have replaced  $t_0$  by 0 in Eq. (16) without loss of generality. The monodromy matrix is obtained using the approach discussed in Section 4.1

From Eq. (16), we can see that  $\mathbf{F}(0)$  is the eigenvector matrix of the monodromy matrix. Moreover,  $\mathbf{J}$  will be diagonal with the Poincaré exponents as its entries;  $\mathbf{J} = \text{diag}[\omega_1 \dots \omega_n]$ .

The Poincaré exponents are the time-periodic equivalents of the eigenvalues for time-invariant system, and are related to the eigenvalues of the monodromy matrix in the following way:

$$\omega_i = \frac{\ln(\Theta_i)}{P} \quad (17)$$

where  $\Theta_i$  represents the  $i$ -th eigenvalues of the monodromy matrix. Since  $\mathbf{F}(t)$  is time-periodic and therefore bounded, the stability of the system depends solely on the Poincaré exponents and those are now known from Eq. (17). At this stage, we have all the knowledge to assess the stability of the system, but not enough to design controllers. As will be shown in Section 4.3, we now need to compute matrix  $\mathbf{F}(t)$  to allow design of the controller. With the matrix  $\mathbf{J}$  known,  $\mathbf{F}(t)$  can be obtained for all time by rearranging Eq. (11)

$$\mathbf{F}(t) = \mathbf{\Phi}(t,0)\mathbf{F}(0)e^{-\mathbf{J}P} \quad (18)$$

It is important to note that there is no guarantee that the Floquet factors will be real using this method. Real Floquet factors are desirable because the control gain matrix is a function of the Floquet factors. An appropriate rearrangement exists that makes both matrices real and leaves the previous formula unaltered (Calico and Weisel 1984). The result is that the Floquet factors are real and Eqs. (11)-(16) still hold.

#### 4.3 Control laws: theory

In the previous sections, we have shown how to obtain the state-transition matrix and the Floquet factors for a system in the form of Eq. (8). We now have all the tools to design control laws for our time-periodic system. We first introduce another variable that we call the modal variable

$$\boldsymbol{\eta}(t) = \mathbf{F}^{-1}(t)\mathbf{x}(t) \quad (19)$$

We can then rewrite Eq. (8) in terms of the modal variable

$$\dot{\boldsymbol{\eta}}(t) = \mathbf{J}\boldsymbol{\eta}(t) + \mathbf{F}^{-1}(t)\mathbf{B}(t)\mathbf{u}(t) \quad (20)$$

This means that the matrix  $\mathbf{F}(t)$  reduces the time-periodic system of Eq. (8) into a constant-coefficient system. We will use a simple proportional feedback for our control law

$$\mathbf{u}(t) = \mathbf{K}(t)(\boldsymbol{\eta}_d(t) - \boldsymbol{\eta}(t)) \quad (21)$$

where the subscript  $d$  denotes a desired value and  $\mathbf{K}(t)$  is a  $6 \times 12$  control gain matrix. Using this control law, the system described by Eq. (20) becomes

$$\dot{\boldsymbol{\eta}}(t) = [\mathbf{J} - \mathbf{F}^{-1}(t)\mathbf{B}(t)\mathbf{K}(t)]\boldsymbol{\eta}(t) + \mathbf{F}^{-1}(t)\mathbf{B}(t)\mathbf{K}(t)\boldsymbol{\eta}_d(t) \quad (22)$$

The first part of Eq. (22) is the controller natural response of the system. The eigenvalues of  $\mathbf{J} - \mathbf{F}^{-1}(t)\mathbf{B}(t)\mathbf{K}(t)$  are different from those of  $\mathbf{J}$  in Eq. (20) and are determined by the gain matrix  $\mathbf{K}(t)$ . By adjusting the gain matrix, the eigenvalues can be selected to improve the response of the system. The second part of Eq. (22) determines how the system will track a desired trajectory. Now, we can define the  $12 \times 6$  controllability matrix

$$\mathbf{G}(t) = \mathbf{F}^{-1}(t)\mathbf{B}(t) \quad (23)$$

In our case, since we only have direct control over the velocity states, the controllability matrix will have a maximum rank of 6. Then, the matrix of Poincaré exponents of the controlled system is given by

$$\mathbf{J}' = \mathbf{J} - \mathbf{G}(t)\mathbf{K}(t) \quad (24)$$

The control problem here becomes finding the appropriate gain matrix  $\mathbf{K}(t)$  that will place the poles at the desired locations. It is also important to note that since  $\mathbf{G}(t)$  has a rank of 6, only 6 eigenvalues can be selected independently. Calico and Weisel (1984) proposed a method to determine which eigenvalues to modify. The  $\mathbf{J}$  matrix is partitioned into modes to control and modes to ignore:  $\mathbf{J}_c$  and  $\mathbf{J}_i$

$$\mathbf{J} = \begin{bmatrix} \mathbf{J}_i & \mathbf{0} \\ \mathbf{0} & \mathbf{J}_c \end{bmatrix} \quad (25)$$

The partitioning shown in Eq. (25) is straightforward since  $\mathbf{J}$  is almost diagonal. Therefore, moving the rows will not affect the column. The same row operations were applied to  $\mathbf{G}(t)$ ,  $\mathbf{K}(t)$ , and  $\boldsymbol{\eta}(t)$

$$\mathbf{G}(t) = \begin{bmatrix} \mathbf{G}_i(t) \\ \mathbf{G}_c(t) \end{bmatrix} \quad \mathbf{K}(t) = [\mathbf{K}_i(t) \quad \mathbf{K}_c(t)] \quad \boldsymbol{\eta}(t) = \begin{bmatrix} \boldsymbol{\eta}_i(t) \\ \boldsymbol{\eta}_c(t) \end{bmatrix} \quad (26)$$

where  $\mathbf{G}_c(t)$ ,  $\mathbf{G}_i(t)$ ,  $\mathbf{K}_c(t)$  and  $\mathbf{K}_i(t)$  are  $6 \times 6$  matrices and  $\boldsymbol{\eta}_c(t)$  and  $\boldsymbol{\eta}_i(t)$  are  $6 \times 1$  vectors. Then, the first part of Eq. (22) becomes (Calico and Weisel 1984)

$$\begin{bmatrix} \dot{\boldsymbol{\eta}}_c(t) \\ \dot{\boldsymbol{\eta}}_i(t) \end{bmatrix} = \begin{bmatrix} \mathbf{J}_i - \mathbf{G}_i(t)\mathbf{K}_i(t) & -\mathbf{G}_i(t)\mathbf{K}_c(t) \\ -\mathbf{G}_c(t)\mathbf{K}_i(t) & \mathbf{J}_c - \mathbf{G}_c(t)\mathbf{K}_c(t) \end{bmatrix} \begin{bmatrix} \boldsymbol{\eta}_i(t) \\ \boldsymbol{\eta}_c(t) \end{bmatrix} \quad (27)$$

By setting  $\mathbf{K}_i(t)$  to  $\mathbf{0}$ , the controlled modes can be decoupled from the uncontrolled ones. Furthermore, this leaves the eigenvalues of the ignored modes unchanged. Rewriting Eq. (24) for the controlled modes

$$\mathbf{J}'_c = \mathbf{J}_c - \mathbf{G}_c(t)\mathbf{K}_c(t) \quad (28)$$

where  $\mathbf{J}'_c$  is the desired eigenvalues matrix. With  $\mathbf{G}_c(t)$  being a square full rank matrix, we can find the required control gains to place the poles at the desired location

$$\mathbf{K}_c(t) = \mathbf{G}_c^{-1}(t)[\mathbf{J}'_c - \mathbf{J}_c] \quad (29)$$

and the full gain matrix is given by

$$\mathbf{K}(t) = [\mathbf{K}_c(t) \quad \mathbf{0}] \quad (30)$$

Finally, the gain matrix in the  $\mathbf{x}(t)$  domain can be obtained by post-multiplying Eq. (29) by  $\mathbf{F}^{-1}(t)$ .

#### 4.4 Floquet control laws: application

In this section, we describe how the theory discussed in the preceding sections was applied to the Aqua vehicle. The state-transition matrix was obtained using the single-pass approach developed by Cai *et al.* (2001), discussed in Section 4.1.

The complete design process to go from the nonlinear dynamics model to the gain matrix is presented in Fig. 7. The model is first linearized using the technique described in Section 3. This technique has the advantage of giving  $\mathbf{A}(t)$  as a sum of a constant term and a sinusoidal term, which allows using Eqs. (12) and (13) directly. Then, the state-transition matrix is computed with results from Section 4.1 while the Floquet factors are obtained using the procedure detailed in Section 4.3. Finally, the control gain matrix can be obtained from the Floquet factors to achieve a desired performance.

The linearization of the vehicle for this controller was performed at a speed of approximately  $u = 0.5$  m/s. The paddle period and amplitude of oscillation to obtain that speed are  $P = 0.4$  s and  $A = 0.6$  rad. The speed in all other degrees of freedom was zero.

Matrix  $\mathbf{J}$  was initially diagonal but some of its entries were complex. The method of Calico and Weisel (1984) was used to eliminate the complex part of  $\mathbf{J}$  but as a result,  $\mathbf{J}$  has some off-diagonal elements.

The second factor,  $\mathbf{F}(t)$ , is time-varying and periodic with period  $P$ . However, as we can see from Eqs. (19) and (23) the inverse of  $\mathbf{F}(t)$  is in fact more relevant for use in the controller. Similarly to  $\mathbf{A}(t)$ , it is composed of a constant term and of a sinusoidal term

$$\mathbf{F}^{-1}(t) = \mathbf{a}_F + \mathbf{K}_F \cos\left(\frac{2\pi}{P}t\right) \quad (31)$$

$\mathbf{F}^{-1}(t)$  is known and each entry is taken individually and decomposed into its constant (average) value and its oscillating term. The first thing to notice from these matrices is that the constant term is generally more dominant than the sinusoidal term. Eq. (31) gives us  $\mathbf{F}^{-1}(t)$  at any time. However, it is more convenient in practice to have this matrix as a function of the paddle position since the periodicity of the system comes from the oscillating paddles. Noting that the paddle angle is sinusoidal, we can obtain an equation for  $\cos\left(\frac{2\pi}{P}t\right)$  as a function of the paddle angle ( $\gamma$ )

$$\cos\left(\frac{2\pi}{P}t\right) = \frac{\gamma(t) - \lambda}{A} \quad (32)$$

where  $A$  is the amplitude of oscillation of the paddle and  $\lambda$  is the paddle offset angle. We can combine Eqs. (31) and (32) to obtain an expression for  $\mathbf{F}^{-1}(t)$  that depends only on paddle

position  $\gamma(t)$

$$\mathbf{F}^{-1}(t) = \mathbf{a}_F + \mathbf{K}_F \frac{\gamma(t) - \lambda}{A} \tag{33}$$

Using Eq. (32) is convenient because the paddle angle is measured on the actual robot. With both Floquet factors known, the next step is to determine an appropriate  $\mathbf{J}'_c$  for our system. By altering the pole locations, we can achieve different performance. Our objective was to obtain a critically damped system and therefore the fastest response. Table 1 is used to appropriately tune the eigenvalues to obtain the desired performance. It is based on  $\mathbf{F}^{-1}(t)$  which relates  $\mathbf{x}(t)$  to  $\boldsymbol{\eta}(t)$ . Since  $\mathbf{a}_F$  represents the average value of  $\mathbf{F}^{-1}(t)$ , Table 1 is obtained from inspection of  $\mathbf{a}_F$ . Any significant entry  $a_{ij}$  tells us that  $\eta_i$  has a significant effect on  $x_j$ . Table 1 summarizes the inspection of  $\mathbf{a}_F$ . As we can see,  $x_3(t)$  and  $x_6(t)$  each appear three times in the bottom row of Table 1, which means that their tuning is not straightforward. Moreover, as was mentioned in the previous section, we cannot control all 12 degrees of freedom independently because our controllability matrix  $\mathbf{G}(t)$  is only of rank 6. However, since some states of the modal variable depend on multiple states of the vehicle, we can actually control more than 6 states, though not independently. The most obvious choice for the controlled states are  $\eta_1(t)$ -  $\eta_6(t)$  since this will allow control of 11 of the 12 states of the vehicle. The only uncontrolled state is the fourth one, the roll rate. However, the roll motion is controlled by  $x_{10}$ , the roll angle.

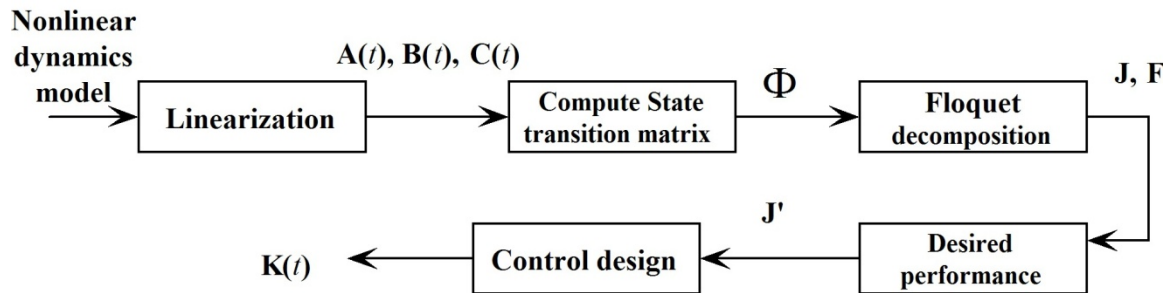


Fig. 7 Flowchart of the process to obtain the control gain matrix

Table 1 Relationship between the original states and the modal variable states

$\boldsymbol{\eta}(t)$	1	2	3	4	5	6	7	8	9	10	11	12
$\mathbf{x}(t)$	1, 7	6, 8	3, 9	10	3, 5, 11	2, 12	1	5	3	2, 6	2, 6	4

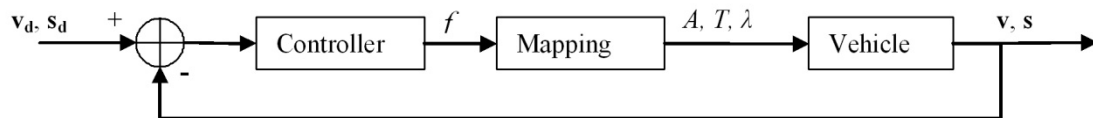


Fig. 8 Control loop

## 5. Results

In this section, we present the performance of the controllers that were presented in Section 4. The performance was first assessed in simulation and then experimentally. The simulation is based on the model described in Section 2 and is implemented in the MATLAB Simulink environment using the standard control loop shown in Fig. 8. We can see that the input to the system is the desired trajectory. The controller outputs the desired force in the six degrees of freedom, then the reverse mapping transforms this force into an amplitude, period and offset ( $\lambda$ ) of oscillation of each paddle.

In order to demonstrate that treating Aqua as a time-periodic system using Floquet control has advantages, we compared its performance to that of a simple PD controller. The Floquet controller was designed by setting the desired eigenvalues to obtain a critically damped system, and then using Eq. (29) to obtain the control gain matrix. On the other hand, the PD controller gains were tuned by trial and error based on experience acquired in previous experimental tests.

### 5.1 Simulation results

The simulation described in Section 2 is used to perform an initial assessment of the performance of the controllers, and to properly tune the control gains. Simulations are run in which the vehicle must follow a prescribed trajectory. Five maneuvers that cover the most general motion of the vehicle were defined: roll angle ramp, sinusoidal roll angle, roll angle pulses, pitch angle pulses and finally a sinusoidal pitch angle.

The simulation results are shown in Figs. 9 and 10. We can clearly see that both controllers provide good trajectory tracking capabilities to the vehicle. Their performance is very similar and the only apparent advantage of the Floquet controller is in step tracking where its settling time is slightly smaller than for the PD controller. Based on these simulation results we expect good tracking for all maneuvers during the experiment.

### 5.2 Experimental results

In this section, we present the results of the experiment in which we tested the PD and Floquet controllers.

Fig. 11 shows the general setup used when performing experiments with Aqua. The upper

figure is a schematic of the set of the equipment and the lower portion of the figure shows an actual setup used during an experiment (Chiu *et al.* 2013). The vehicle is connected to the Operator Control Unit (OCU) through an optical fiber. The OCU is then connected to a laptop with a serial cable. There is a monitor on top of the OCU that displays the images captured by the camera onboard Aqua. All the information related to the state of the vehicle is transmitted to the laptop.

The pilot sees the actual and desired state of the vehicle on the GUI shown in Fig. 12. The pilot controls the vehicle using a gamepad also shown in Fig. 12. The commands given by the human pilot are also displayed on the GUI.

During our experiments, the roll, pitch and yaw are controlled by our controllers while the speed remains in control of the operator. However, the speed was not changed in this set of experiments. We operated from a boat that was approximately 300 m offshore so that the surf did not interfere with the experiments. The water was quite rough and there was significant water current. We tried to align the vehicle with the current to minimize the disturbance.

Aqua sensors can only measure the Euler angles accurately. Sensing of the translational degrees of freedom is inaccurate and cannot be used for feedback purposes. Moreover, the compass that measures the heading of the vehicle is somewhat unreliable and as a result only pitch and roll motion were tested during this experiment. The maneuvers used were the same as in the simulation.

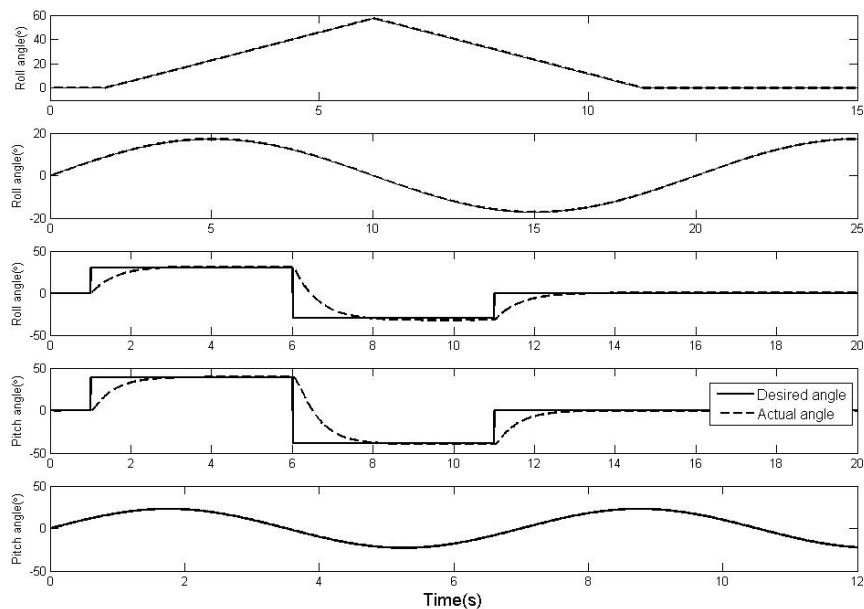


Fig. 9 Performance of the Floquet controller in the simulation

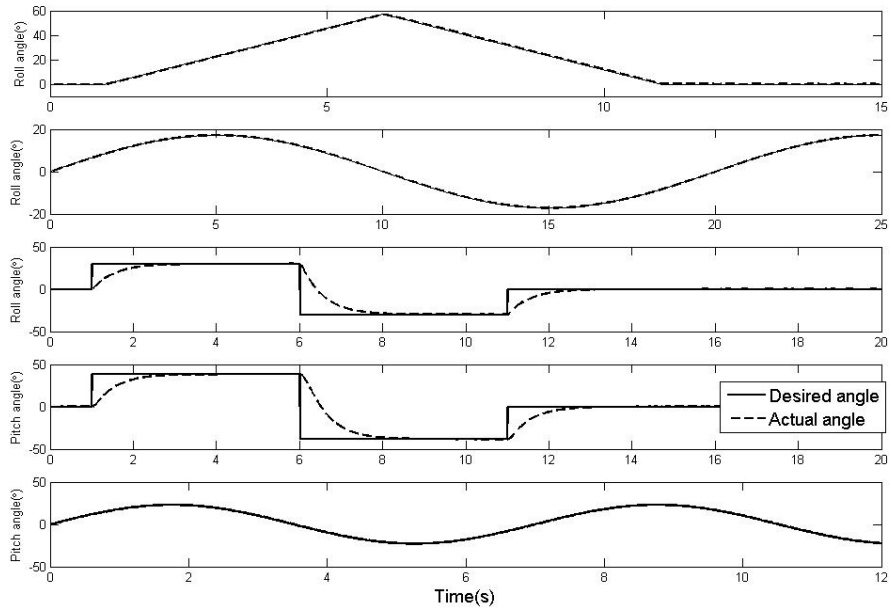


Fig. 10 Performance of the PD controller in the simulation



Fig. 11 General experimental setup with Aqua

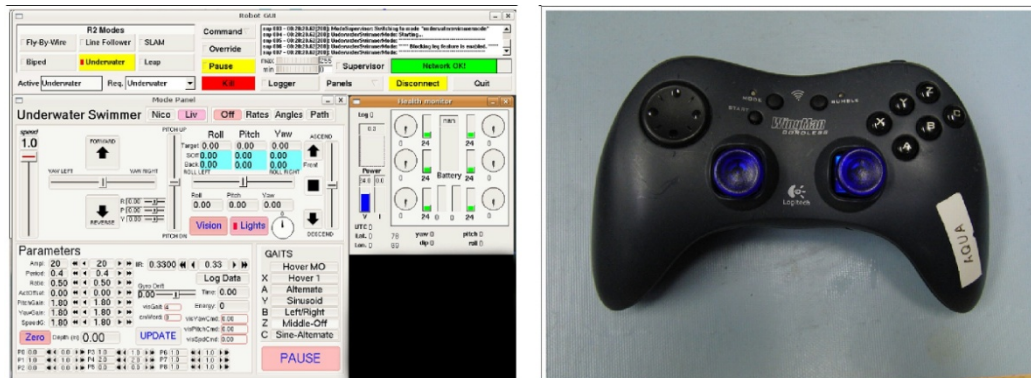


Fig. 12 Input devices. (a) Graphical User Interface(GUI) and (b) Gamepad

Figs. 13 and 14 show how the two controllers were able to track the different trajectories. The first thing we notice is that both controllers were able to track the trajectory with reasonable accuracy, especially in roll angle. Moreover, we see that the Floquet controller gives a better performance in the roll angle ramp experiment. However, it is important to note that the PD controller was tuned to give good performance for these maneuvers while the Floquet controller did not require any tuning. It is possible that, through adjustment of the eigenvalues of  $\mathbf{J}'$ , the performance of the Floquet controller could be improved further.

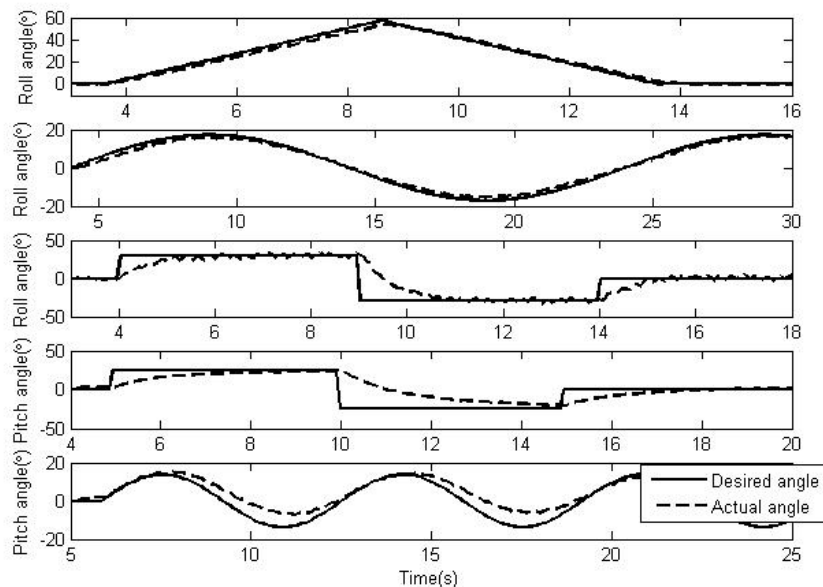


Fig. 13 Performance of the Floquet controller in the experiment

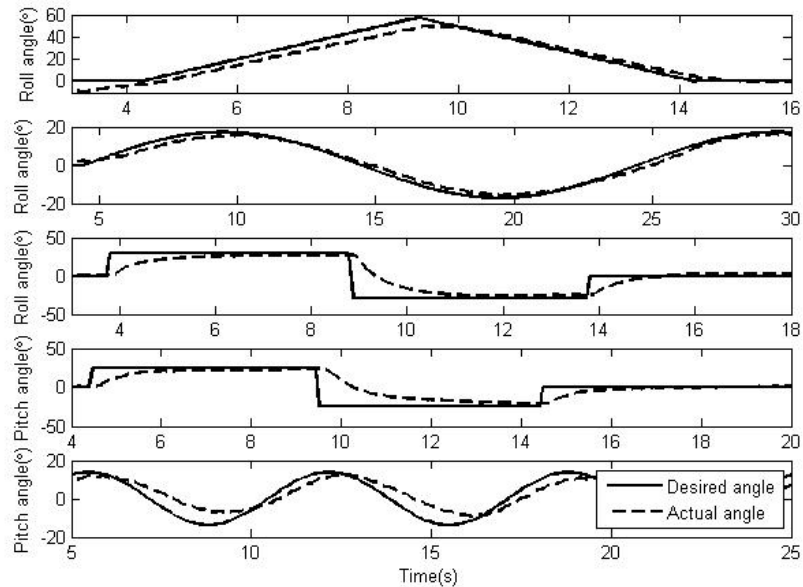


Fig. 14 Performance of the PD controller in the experiment

We can also notice from the two figures that the tracking is significantly better in roll than it is in pitch. There are two main reasons to explain this phenomenon. First, the moment of inertia is larger in pitch than it is in roll. Therefore, more force needs to be applied to produce the same motion. Second, only four paddles can actively produce a pitch moment while all six paddles can contribute to the roll moment. This is due to the fact that the two middle paddles are close to the y-axis of the vehicle.

Based on the results shown in Figs. 13 and 14, we can conclude that our controllers provide good trajectory tracking capabilities to Aqua. Moreover, although the PD controller gives good performance, it requires tuning which was not necessary with the Floquet controller.

## 6. Conclusions

This paper describes the design of Floquet controllers for trajectory tracking of a biomimetic underwater vehicle. A linearized time-varying model of the vehicle was developed to provide a basis for the controller design. From that model, the relevant state transition matrix and Floquet factors were found using existing methods. A proportional feedback gain matrix was then derived using the Floquet factors. The performance of the resulting controller was first evaluated using a nonlinear simulation of the vehicle, and compared to the performance of a more traditional PD controller. It was found that the Floquet controller performed slightly better in response to step input commands. An experiment was then performed to validate the performance of the Floquet controller design in an open dynamic environment and compared to the PD controller. The results

indicated that, while both controllers were able to provide trajectory tracking capabilities, the Floquet controller slightly outperformed its PD counterpart especially in the roll ramp experiment. Moreover, the Floquet controller has the advantage of requiring no tuning. In the future, experiments in a controlled environment will be done to allow a more systematic evaluation of controller performance. It would also be useful to improve the sensing capability of the vehicle, and the test environment, so that a greater range of maneuvers can be accurately tested.

## References

- Acho, L., Orlov, Y. and Solis, V. (2001), "Nonlinear measurement feedback  $H_\infty$  control of time-periodic systems with application to tracking control of robot manipulators", *Int. J. Control*, **74**, 190-198.
- Brocket, R. (1970), *Finite dimensional linear systems*, New-York, Wiley.
- Cai, Z., Gu, Y. and Zhong, W. (2001), "A new approach computing Floquet transition matrix", *Comput. Struct.*, **79**(6), 631-635.
- Calico, R. and Wiesel, W. (1984), "Control of time-periodic systems", *J. Guidance*, **7**, 671-676.
- Chiu, O., Nahon, M. and Plamondon, N. (2013), "Stability augmentation and fault tolerance for a hexapod underwater vehicle", *Marine Eng. Frontiers*, **1**, 1-12.
- Fossen, T. (1994), *Guidance and control of ocean vehicle*, United Kingdom: John Wiley and Sons Ltd.
- Geder, J., Palmisano, J., Ramamurti, R., Sandberg, W. and Ratna, B. (2008), "Fuzzy logic PID based control design and performance for a pectoral fin propelled unmanned underwater vehicle", *Proceedings of the 2008 International Conference on Control, Automation and Systems*, Seoul, South Korea.
- Georgiades, C., Nahon, M. and Buehler, M. (2009), "Simulation of an underwater hexapod robot", *Ocean Eng.*, **36**(1), 39-47.
- Guo, J. and Joeng, Y.J. (2004), "Guidance and control of biomimetic autonomous underwater vehicle using body-fin propulsion", *Proceedings of the institute of Mechanical Engineers Part M: J. Eng. Maritime Environ.*, **218**(2), 93-111.
- Montagnier, P., Spiteri, R.J. and Angeles, J. (2004), "The control of linear time-periodic systems using Floquet-Lyapunov theory", *Int. J. Control*, **17**, 472-490.
- Maik, M. and Singh, S. (2007), "Oscillatory adaptive yaw-plane control of biorobotic autonomous underwater vehicles using pectoral-like fins", *Appl. Bionics Biomech.*, **4**(4), 137-147.
- Plamondon, N. and Nahon, M. (2006), "A flexible oscillating foil model for an underwater auv", *Proceedings of the CANCAM 2006*, Toronto, Ontario.
- Plamondon, N. and Nahon, M. (2009), "A trajectory tracking controller for an underwater hexapod vehicle", *Bioinspir. Biomim.*, **4**(3), 036005 doi:10.1088/1748-3182/4/3/036005.
- Smallwood, D. and Whitcomb, L. (2004), "Model based dynamic positioning of underwater robotic vehicles: theory and experiment", *IEEE J. Ocean Eng.*, **29**(1), 169-186.
- Xu, H., Mirmirami, M., Ioannou, P. and Boussalis, H. (2001), "Robust adaptive sliding control of linearizable systems", *Proceedings of the 2001 American Control Conference*.
- Yoerger, D. and Slotine, J.J.E. (1985), "Robust trajectory control of underwater vehicles", *IEEE J. Ocean Eng.*, **10**(4), 462-470.